NANO LETTERS

2007
Vol. 7, No. 4
1032−1036

Synthesis and Optical Properties of Silver Nanobars and Nanorice

Benjamin J. Wiley,[†] Yeechi Chen,[‡] Joseph M. McLellan,[‡] Yujie Xiong,[‡] Zhi-Yuan Li,[§] David Ginger,[‡] and Younan Xia*[,‡]

Department of Chemical Engineering and Department of Chemistry, University of Washington, Seattle, Washington 98195, and Institute of Physics, Chinese Academy of Sciences, Beijing 100080, People's Republic of China

Received January 26, 2007; Revised Manuscript Received February 21, 2007

ABSTRACT

Silver nanobars with rectangular side facets and an average aspect ratio of 2.7 have been synthesized by modifying the concentration of bromide added to a polyol synthesis. Subsequent rounding of nanobars transformed them into nanorice. Due to their anisotropy, nanobars and nanorice exhibit two plasmon resonance peaks, scattering light both in the visible and in the near-infrared regions. With a combination of discrete-dipole approximation calculations and single-nanoparticle spectroscopy, we explored the effect of nanostructure aspect ratio and corner sharpness on the frequency of plasmon resonance. Near-field calculations and surface-enhanced Raman scattering measurements on single particles were performed to show how local field enhancement changes with both the wavelength and polarization of incident light.

Particles of silver and gold an order of magnitude smaller than the wavelengths of visible light strongly scatter and absorb light due to surface plasmon resonance, the collective oscillation of conduction electrons induced by incident light. The frequency and intensity of plasmon resonance are dependent on the distribution of polarization charge across the nanostructure, which is in turn determined by its shape.[1] Thus, to control the shape of a metal nanostructure is to control the wavelengths of light it scatters and absorbs, as well as the degree to which it enhances local electric fields.[2,3]

Solution-phase synthesis has proven effective at producing large quantities of nanostructures with controlled shapes and properties.[4−6] Silver and gold have a highly symmetric, face-centered cubic crystal structure, but many anisotropic shapes can be grown by controlling the assembly of metal atoms in solution. The synthesis and properties of gold nanorods have garnered particular attention primarily because the color of light they scatter can be tuned from the visible to the near-infrared (NIR) regions simply by controlling their aspect ratio.[7−10] Because gold nanorods absorb and scatter light in the NIR region, where absorbance of light by biological tissue is at a minimum, they can potentially be used for optical imaging and photothermal therapy of cancer.[11,12]

In contrast to gold, study of the synthesis and optical properties of silver nanorods is limited. This is despite the fact that nanoparticles of silver less than 60 nm in diameter scatter light with twice the efficiency of gold and are 2 orders of magnitude better at enhancing the Raman signals of adsorbed molecules.[13,14] To date, only one synthesis was able to generate significant quantities of silver nanorods with transverse and longitudinal plasmon peaks. This synthesis involved production of silver seeds by reducing $AgNO_3$ with $NaBH_4$ in the presence of citrate, followed by growth of the seeds into nanorods in the presence of ascorbic acid and cetyltrimethylammonium bromide (CTAB).[15] A mixture of spheres and rods was produced, and the rods had to be purified by centrifugation. The longitudinal resonance of nanorods produced by this method has not been tuned past ~700 nm.

Here we report the synthesis of silver nanobars that scatter and absorb light in both the visible and NIR regions. Like nanorods, nanobars grow anisotropically, with an average aspect ratio of 2.7 (146 nm long, 56 nm wide). Unlike nanorods, nanobars are single crystals bounded by (100) facets and thus have the sharp corners and edges of a nanocube. In a postsynthesis step, the corners and edges of the nanobars can be rounded to transform them into single-crystal nanorice. Thus we can study not only the relationship between aspect ratio and the frequency of plasmon resonance but concurrently the influence of corner sharpness. In addition, we have studied the effect of polarization on local field enhancement with a combination of near-field calculations and surface-enhanced Raman scattering (SERS) on single nanoparticles.

* Corresponding author. E-mail: xia@chem.washington.edu.
[†] Department of Chemical Engineering, University of Washington.
[‡] Department of Chemistry, University of Washington.
[§] Institute of Physics, Chinese Academy of Sciences.

10.1021/nl070214f CCC: $37.00
Published on Web 03/08/2007

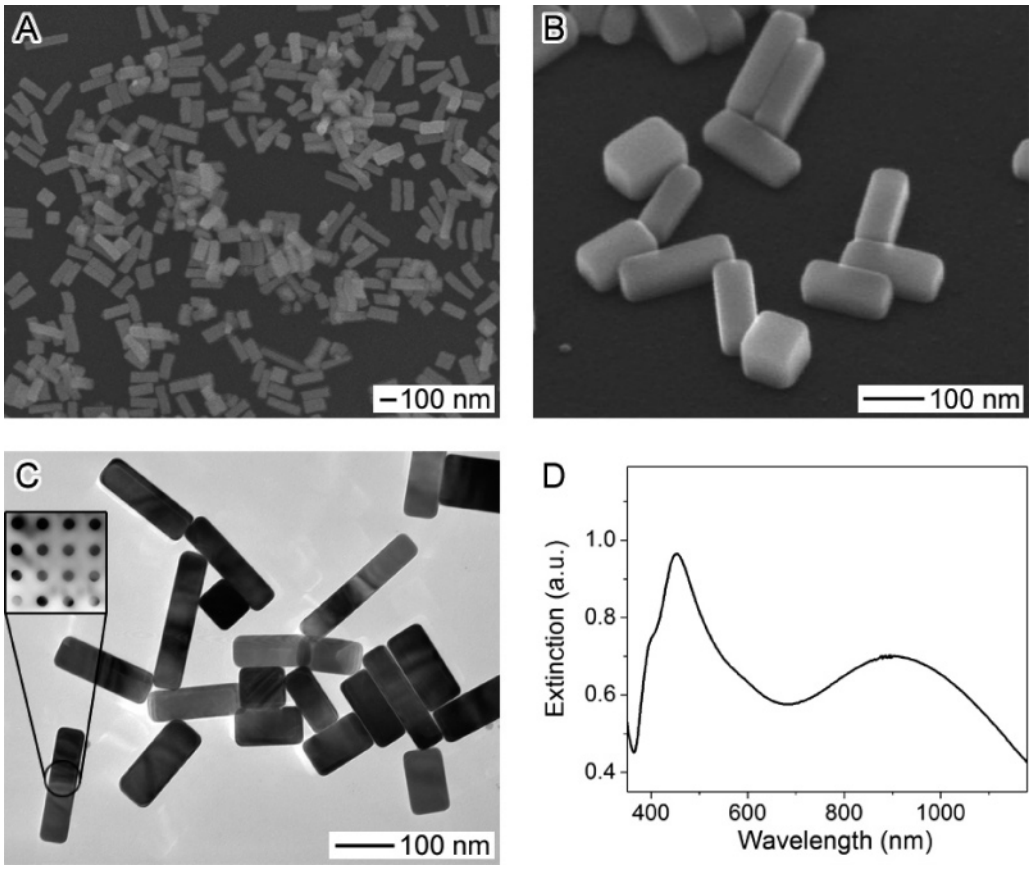

Figure 1. (A) SEM image of silver nanobars. (B) SEM image of the same sample tilted by 45°. (C) TEM image of the silver nanobars. The inset is a convergent beam electron diffraction pattern, indicating the nanobars are single crystals bounded by (100) facets. (D) The vis−NIR extinction spectrum of nanobars is characterized by a transverse plasmon resonance in the visible and a longitudinal resonance in the near-infrared region.

As with silver nanocubes, bipyramids, pentagonal nanowires, and nanobeams, synthesis of nanobars relies on the polyol synthesis in which ethylene glycol (EG) serves as both solvent and reducing agent.[16−20] To start the synthesis, two solutions, one containing 48 mg of $AgNO_3$ in 3 mL of EG, the other containing 48 mg of poly(vinyl pyrrolidone) (PVP) and 0.068 mg of NaBr in 3 mL of EG, were added dropwise via a two-channel syringe pump into 5 mL of EG heated in an oil bath at 155 °C. The reaction was stopped after 1 h, at which time the solution contained a mixture of nanocubes and nanobars with a range of aspect ratios.

The scanning electron microscopy (SEM) image in Figure 1A shows an area covered with silver nanobars of varying proportions. By tilting the sample 45°, as has been done in Figure 1B, one can better observe the shape of the nanobar. In this image it appears nanobars are both narrower and thinner than nanocubes in the same sample. Figure 1C is a TEM image of the silver nanobars. To determine their side facets and crystallinity, we performed convergent beam electron diffraction on several of the nanobars. All patterns were essentially the same as the one included as an inset, which shows diffraction from the (100) planes. As all sides of the nanobars meet at right angles, these patterns prove nanobars, like nanocubes, are single crystals bounded on all sides by (100) facets.

Given that every side of the nanobar has the same surface energy, the question arises as to how and why the nanobars grew anisotropically. The most important ingredient for promoting the growth of nanobars relative to other shapes is bromide. We previously employed bromide at low concentrations (Ag:Br = 850) to selectively etch away multiply twinned seeds, leaving seeds with a single twin intact to grow and form right bipyramids.[18] For the synthesis of nanobars, the concentration of bromide was doubled relative to the synthesis of right bipyramids. The higher concentration of bromide could enhance etching, leading to the production of single crystals. In support of this hypothesis, we found the extinction peak of silver nanoparticles decreased when the concentration of bromide was doubled (Figure S1), presumably due to increased etching by bromide. In addition to promoting production of single-crystal seeds, oxidative etching could cause anisotropic growth if it removed material from one side of the seed more than others. We have previously observed that corrosion of silver nanocubes in the presence of $HAuCl_4$ occurs from only one side by a pitting process, even though all sides have the same (100) atomic packing.[21] More recent results show etching with high concentrations of bromide (Br:Pd = 30) promotes formation of palladium nanorods in the presence of PVP.[22] However, as numerous studies on the growth mechanism of

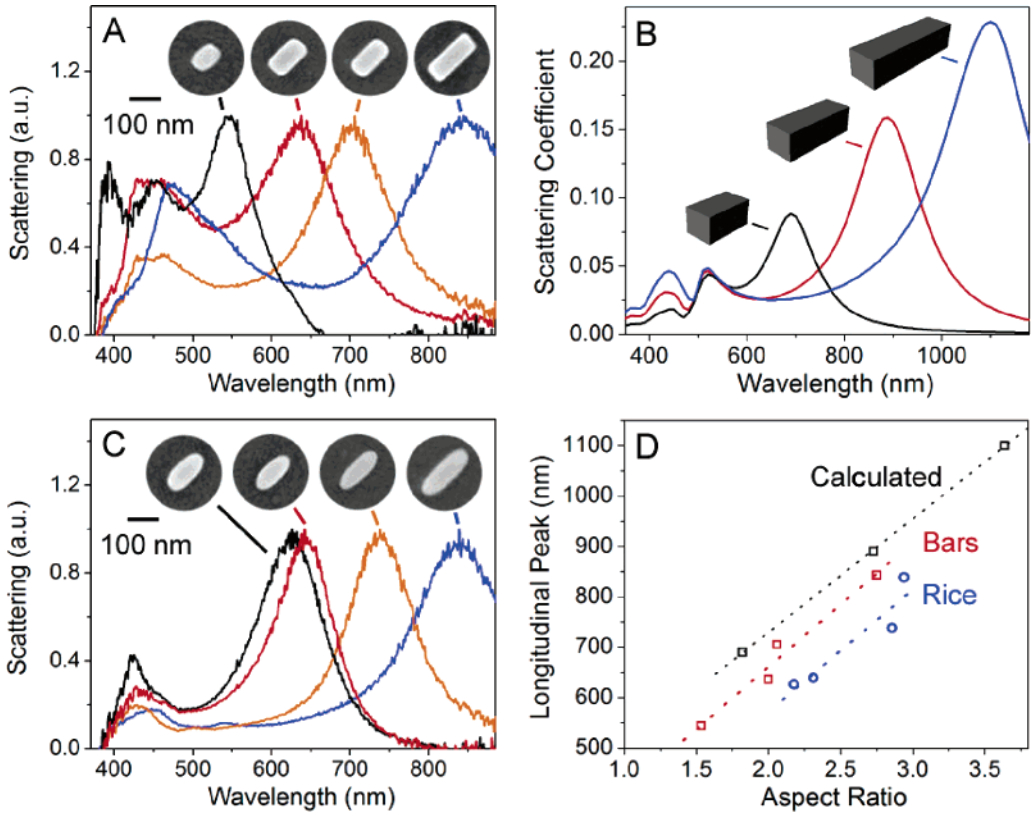

Figure 2. (A) SEM images of individual nanobars with their corresponding normalized scattering spectra. The longitudinal plasmon peak of nanobars red shifts with increasing aspect ratio. (B) DDA calculated scattering spectra of nanobars 100, 150, and 200 nm in length, keeping width = 55 nm and height = 50 nm. (C) SEM images of individual nanorice with their corresponding normalized scattering spectra. (D) Plot of longitudinal plasmon peak location versus aspect ratio. The peaks of both nanobars and nanorice red shift with increasing length, but on average the peaks of nanobars are 80 nm red-shifted from nanorice.

gold nanorods have demonstrated, translating experimental results into a clear and definitive mechanism is no easy task.[5] Thus, etching may play a role in the growth of nanobars, but it is not clear exactly how this occurs, or whether other factors are inducing anisotropic growth.

A fascinating feature of nanobars is their optical properties. The visible−NIR extinction spectrum taken from a suspension of the as-obtained nanobars is characterized by two resonance peaks, one in the blue region of the visible spectrum at 460 nm and the other in the NIR centered at 900 nm (Figure 1D). The plasmon resonance in the visible comes from nanobars polarized along their short axis (transverse plasmon resonance), with some additional contribution from nanocubes in the product. The resonance in the NIR comes from nanobars polarized along their long axis (longitudinal plasmon resonance). Both resonance features are quite broad due to the diversity of nanobar lengths and widths.

The extinction peaks were assigned to particular resonances based on the discrete dipole approximation (DDA) calculations shown in Figure S2.[23,24] For nanobars with aspect ratios of 2, 3, or 4, transversely polarized light is scattered and absorbed in the visible region, with a slight increase in intensity for nanobars with greater aspect ratios. In contrast, the scattering and absorption of longitudinally polarized light are highly dependent on nanobar aspect ratio. The resonance peak position shifts from 700 to 1100 nm, and light scattering doubles in intensity as the aspect ratio of the nanobars increases from 2 to 4.

The dependence of the optical properties on shape was explored experimentally by performing single nanoparticle spectroscopy on nanobars with different aspect ratios. In this experiment, nanobars were sparsely dispersed on glass slides coated with indium tin oxide, and SEM images were taken to record the sizes, shapes, and locations of nanobars on the substrate. Individual nanobars imaged with SEM were then located under an optical microscope. A standard tungsten halogen lamp coupled to a dark field condenser was used for transmitted dark field illumination, and the light scattered from each nanostructure was directed via a fiber optic cable to a charge coupled device spectrometer.

The normalized scattering spectra of individual nanobars are plotted in Figure 2A, with insets giving SEM images of the nanobars from which the scattered light was collected. As predicted by the DDA calculations, the position of the transverse resonance peak stays relatively constant, while the longitudinal resonance peak red shifts with increasing aspect ratio. The transverse peak of the shortest nanobar appears to be split, with an additional sharp peak just below 400 nm. This resonance splitting was previously observed for nanocubes supported on a glass substrate, with the blue-shifted peak associated with strong fields away from the substrate and the red-shifted peak associated with strong

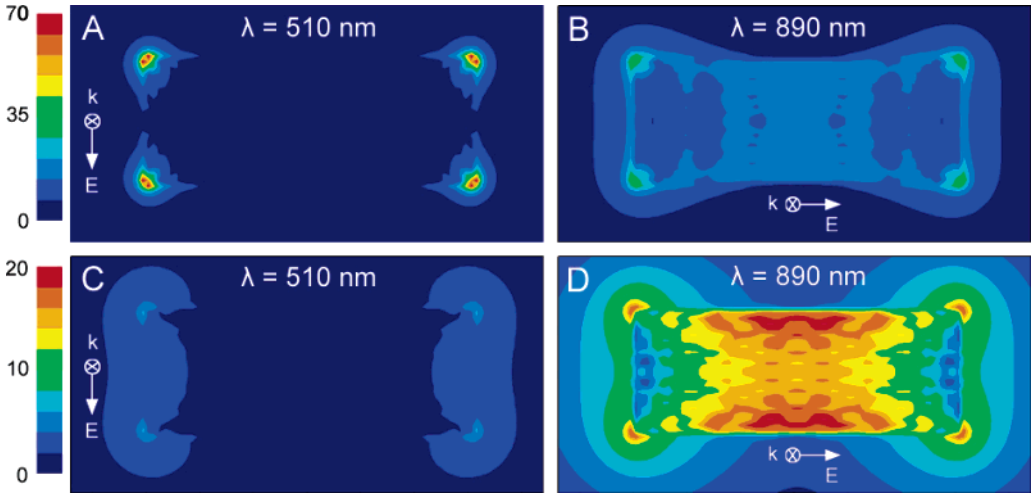

Figure 3. Plots of the relative field amplitude around (A, B) the front and (C, D) the center of a nanobar 150 nm in length, 55 nm in width, and 50 nm in thickness at its two resonance frequencies. Although the top corners exhibit the maximum field enhancement for transversely polarized light at $\lambda = 510$ nm, the nanobar gives a higher average enhancement for longitudinally polarized light at $\lambda = 890$ nm. The average enhancement of $|E|$ 1 nm from the nanobar surface is 9.7 at 890 nm and 4.8 at 510 nm.

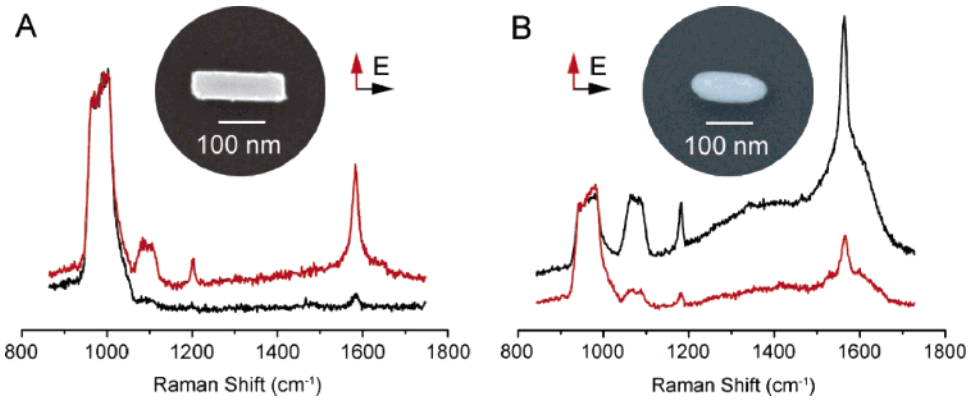

Figure 4. Surface-enhanced Raman spectra from a single (A) nanobar and (B) nanorice covered by a 1,4-benzenedithiol monolayer. Spectra with a transverse 514 nm laser polarization are shown in red and the longitudinal polarization in black. The spectra were normalized to the silicon band between 900 and 1000 nm. For both the nanobar and nanorice, the intensity of SERS enhancement depended on the polarization of incident light.

fields impinging on the glass.[25] This splitting disappears for nanobars with aspect ratios of 2 or more.

The resonance peaks of synthesized nanobars are blue-shifted relative to the calculated scattering spectra of nanobars in Figure 2B. We suspected this shift was caused by the DDA calculations using nanobars with sharper corners and edges than synthesized ones. To further explore the effect of sharpness on resonance peak position, we converted the nanobars into nanorice, a nanostructure with a rounded profile. This conversion was performed by storing the nanobars in a 5 wt % solution of PVP in water at room temperature for 1 week. SEM images of nanorice are given in Figure S3. The normalized scattering spectra of nanorice with different aspect ratios are plotted in Figure 2B, with insets showing SEM images of the nanorice from which the scattered light was recorded. Similar to nanobars, the position of the transverse resonance peak did not change significantly for nanorice with different aspect ratios, and the longitudinal resonance peak red shifted with increasing aspect ratio. However, the rounded corners and edges of nanorice caused both the transverse and longitudinal resonance peaks to be blue-shifted relative to those of nanobars. The observed red shifting of plasmon resonance with increasing corner sharpness of nanobars is consistent with previous comparisons of sharp and rounded nanocubes and nanoplates.[26,27]

To compare the scattering spectra of individual nanobars and nanorice with the DDA-predicted spectra from ideal nanobars, we plotted the longitudinal resonance peak position versus aspect ratio in Figure 2D. For each case, the longitudinal resonance red shifts linearly with aspect ratio. The DDA calculations on nanobars with ideal corner and edge sharpness exhibit the most red-shifted resonance at a given aspect ratio, followed by the nanobars and then nanorice. The peaks of nanobars are on average red-shifted by 80 nm from those of nanorice.

We have shown that the transverse mode scatters light in the visible and the longitudinal mode scatters light in the NIR, but not where electrons are oscillating within the nanobar at these resonance frequencies. Figure 3 plots the calculated relative field amplitude $\{|E|\}/\{|E_0|\}$, where $|E|$ is the local amplitude and $|E_0|$ is the incident amplitude, around a nanobar 150 nm in length, 55 nm in width, and 50

nm in thickness at its two resonance frequencies. For a nanobar illuminated with transversely polarized 510 nm light (panels A and C of Figure 3), polarization is largely confined to the corners and ends of the nanobar with a maximum relative amplitude of 70. This picture of resonance helps to explain why the associated plasmon peak was more affected by changes in corner sharpness than aspect ratio. A nanobar illuminated with longitudinally polarized 510 nm light exhibits little near-field enhancement (Figure S4), with an average field enhancement of 2.

A different picture of resonance appears when the nanobar is illuminated with longitudinally polarized 890 nm light (panels B and D of Figure 3). The polarization charge is broadly distributed throughout the nanobar in a way that clearly depends on its length. Although the maximum relative amplitude is 20 at 890 nm, the broader charge distribution increases the average enhancement relative to the resonance at 510 nm. By averaging the values of $|E|$ at 6336 points 1 nm from the surface of the nanobar, we determined the average enhancements of $|E|$ to be 9.7 at 890 nm and 4.8 at 510 nm for the longitudinal and transverse polarization, respectively.

Near-field enhancement can also be indirectly measured through SERS because the intensity of Raman scattering from a molecule is roughly proportional to $|E|^4$.[3] Figure 4A shows the SERS spectrum of 1,4-benzendithiol (1,4-BDT) on a single nanobar illuminated by transverse and longitudinally polarized 514 nm laser light. The broad band in the spectra at 900−1000 cm^{-1} can be attributed to the Si substrate and was used as a reference for intensity normalization. The peaks at 1080, 1180, and 1565 cm^{-1} are due to the vibrations of 1,4-BDT.[28] The signal is clearly greater when the laser is transversely polarized. Because the transverse plasmon resonance peak for this nanobar is closer to 514 nm than the longitudinal resonance peak, it makes sense that the near-field, and thus the SERS spectrum, would be more enhanced by transversely polarized 514 nm light. Conversely, the corresponding single nanorice spectrum in Figure 4B exhibits a greater enhancement for the longitudinal polarization. This is perhaps because both its longitudinal and transverse resonance peaks are blue-shifted relative to the nanobar, such that greater near-field enhancement occurs at the longitudinal polarization. As with our calculations, these results show that the intensity of near-field enhancement for nanobars and nanorice depends on the polarization of incident light.

Nanobars and nanorice represent an important addition to the surprising variety of silver nanostructures that can be synthesized using a polyol process. Although their growth mechanism remains a mystery, we have thoroughly characterized how their dimensions affect both the wavelengths of light they scatter and the intensity with which they enhance near-fields for molecular spectroscopy. Further mechanistic exploration may improve synthetic control over nanobar size and aspect ratio. This synthetic control is required before nanobars can compete with gold nanorods and nanocages as a class of contrast agents for optical imaging of cancer.[29]

Acknowledgment. This work was supported in part by GEMSEC (an NSF-supported MRSEC program at the University of Washington) and the NSF (DMR-0451788). Y.X. is a Camille Dreyfus Teacher Scholar (2002−2007). B.W. thanks the UW Center for Nanotechnology for an IGERT fellowship funded by the NSF and NCI. Z.Y.L. has been supported by the National Natural Science Foundation of China (No. 10525419) and the National Key Basic Research Special Foundation of China (No. 2004CB719804). D.S.G. is a Cottrell Scholar of the Research Corporation. D.S.G. and Y.C. acknowledge the support of the UW GEMSEC, the AFOSR, and the NSF (DMR-0449422). This work used the Nanotech User Facility (NTUF) at the UW, a member of the National Nanotechnology Infrastructure Network (NNIN) funded by the NSF.

Supporting Information Available: Detailed descriptions of materials and methods, as well as additional figures. This material is available free of charge via the Internet at http://pubs.acs.org.

References

(1) Kottmann, J. P.; Martin, O. J. F.; Smith, D. R.; Schultz, S. *Phys. Rev. B* **2002**, *64*, 235402.
(2) Kelly, K. L.; Coronado, E.; Zhao, L. L.; Schatz, G. C. *J. Phys. Chem. B* **2003**, *107*, 668.
(3) Haes, A. J.; Haynes, C. L.; McFarland, A. D.; Schatz, G. C.; Van Duyne, R. P.; Zou, S. *MRS Bull.* **2005**, *30*, 368.
(4) Wiley, B. J.; Im, S.-H.; Li, Z.-Y.; McLellan, J. M.; Siekkinen, A.; Xia, Y. *J. Phys. Chem. B* **2006**, *110*, 15666.
(5) Murphy, C. J.; Gole, A. M.; Hunyadi, S. E.; Orendorff, C. J. *Inorg. Chem.* **2006**, *45*, 7544.
(6) Chen, J.; Wiley, B. J.; Xia, Y. *Langmuir* **2007**, ASAP, doi:10.1021/la063193y.
(7) El-Sayed, M. A. *Acc. Chem. Res.* **2001**, *34*, 257.
(8) Murphy, C. J.; Sau, T. K.; Gole, A.; Orendorff, C. J.; Gao, J.; Gou, L.; Hunyadi, S.; Li, T. *J. Phys. Chem. B* **2005**, *109*, 13857.
(9) Kim, F.; Song, J. H.; Yang, P. *J. Am. Chem. Soc.* **2002**, *124*, 14316.
(10) Zweifel, D. A.; Wei, A. *Chem. Mater.* **2005**, *17*, 4256.
(11) Oldenburg, A. L.; Hansen, M. N.; Zweifel, D. A.; Wei, A.; Boppart, S. A. *Opt. Express* **2006**, *14*, 6724.
(12) Huang, X.; El-Sayed, I. H.; Qian, W.; El-Sayed, M. A. *J. Am. Chem. Soc.* **2006**, *128*, 2115.
(13) Yguerabide, J.; Yguerabide, E. E. *Anal. Biochem.* **1998**, *262*, 157.
(14) Arya, K. *Phys. Rev. B* **2006**, *74*, 195438.
(15) Orendoff, C. J.; Gearheart, L.; Jana, N. R.; Murphy, C. J. *Phys. Chem. Chem. Phys.* **2006**, *8*, 165.
(16) Wiley, B.; Herricks, T.; Sun, Y.; Xia, Y. *Nano Lett.* **2004**, *4*, 1733.
(17) Im, S. H.; Lee, Y. T.; Wiley, B.; Xia, Y. *Angew. Chem., Int. Ed.* **2005**, *44*, 2154.
(18) Wiley, B. J.; Xiong, Y.; Li, Z.-Y.; Yin, Y.; Xia, Y. *Nano Lett.* **2006**, *6*, 765.
(19) Wiley, B.; Sun, Y.; Xia, Y. *Langmuir* **2005**, *21*, 8077.
(20) Wiley, B.; Wang, Z.; Wei, J.; Yin, Y.; Cobden, D. H.; Xia, Y. *Nano Lett.* **2006**, *6*, 2273.
(21) Sun, Y.; Xia, Y. *J. Am. Chem. Soc.* **2004**, *126*, 3892.
(22) Xiong, Y.; Cai, H.; Wiley, B. J.; Wang, J.; Kim, M.; Xia, Y. *J. Am. Chem. Soc.*, in press.
(23) Draine, B. T.; Flatau, P. J. *J. Opt. Soc. Am. A* **1994**, *11*, 1491.
(24) Yang, W.-H.; Schatz, G. C.; Van Duyne, R. P. *J. Chem. Phys.* **1995**, *103*, 869.
(25) Sherry, L. J.; Chang, S. H.; Schatz, G. C.; Van Duyne, R. P.; Wiley, B. J.; Xia, Y. *Nano Lett.* **2005**, *5*, 2034.
(26) McLellan, J. M.; Siekkinen, A.; Chen, J.; Xia, Y. *Chem. Phys. Lett.* **2006**, *427*, 122.
(27) Mock, J. J.; Barbic, M.; Smith, D. R.; Schultz, D. A.; Schultz, S. *J. Chem. Phys.* **2002**, *116*, 6755.
(28) Cho, S. H.; Han, H. S.; Jang, D.-J.; Kim, K.; Kim, M. S. *J. Phys. Chem.* **1995**, *99*, 10594.
(29) Hu, M.; Chen, J.; Li, Z.-Y.; Au, L.; Hartland, G. V.; Li, X.; Marquez, M.; Xia, Y. *Chem. Soc. Rev.* **2006**, *35*, 1084.

NL070214F